11-1-2012

Fiber-Tip Fabry-Perot Interferometric Sensor based on a Thin Silver Film

Fawen Guo
University of Nebraska-Lincoln, fawen.guo@yahoo.com

Report Documentation Page

Form Approved
OMB No. 0704-0188

1. REPORT DATE	2. REPORT TYPE	3. DATES COVERED
NOV 2012		**00-00-2012 to 00-00-2012**

4. TITLE AND SUBTITLE	5a. CONTRACT NUMBER
Fiber-Tip Fabry-Perot Interferometric Sensor based on a Thin Silver Film	5b. GRANT NUMBER
	5c. PROGRAM ELEMENT NUMBER
6. AUTHOR(S)	5d. PROJECT NUMBER
	5e. TASK NUMBER
	5f. WORK UNIT NUMBER
7. PERFORMING ORGANIZATION NAME(S) AND ADDRESS(ES) **University of Nebraska-Lincoln,Department of Electrical Engineering,Lincoln,NE,68588**	8. PERFORMING ORGANIZATION REPORT NUMBER
9. SPONSORING/MONITORING AGENCY NAME(S) AND ADDRESS(ES)	10. SPONSOR/MONITOR'S ACRONYM(S)
	11. SPONSOR/MONITOR'S REPORT NUMBER(S)

12. DISTRIBUTION/AVAILABILITY STATEMENT
Approved for public release; distribution unlimited

13. SUPPLEMENTARY NOTES

14. ABSTRACT

15. SUBJECT TERMS

16. SECURITY CLASSIFICATION OF:			17. LIMITATION OF ABSTRACT	18. NUMBER OF PAGES	19a. NAME OF RESPONSIBLE PERSON
a. REPORT	b. ABSTRACT	c. THIS PAGE			
unclassified	**unclassified**	**unclassified**	**Same as Report (SAR)**	**44**	

Fiber-Tip Fabry-Perot Interferometric Sensor based on a Thin Silver Film

by

Fawen Guo

A THESIS

Presented to the Faculty of

The Graduate College at the University of Nebraska

In Partial Fulfillment of Requirements

For the Degree of Master of Science

Major: Electrical Engineering

Under the Supervision of Professor Ming Han

Lincoln, Nebraska

November, 2012

Fiber-Tip Fabry-Perot Interferometric Sensor

based on a Thin Silver Film

Fawen Guo, M.S.

University of Nebraska, 2012

Advisor: Ming Han

Fiber-optic sensors have many advantages, including small size, light weight, immunity to electromagnetic interference, and the capability of remote sensing. Fiber-tip sensors are fabricated on a fiber tip and are the smallest type of fiber-optic sensor. The fiber-tip sensors have attracted a great deal of attention in past years for pressure, temperature, and acoustic sensing.

In this thesis, a fiber-tip sensor based on an ultra-thin silver film was proposed and demonstrated for highly sensitive and high frequency ultrasonic detection. The film is prepared by the vacuum thermal deposition method and then transferred to the fiber tip. The sensor has a 300 nm thick film with an inner diameter of 75 μm, corresponding to a static pressure sensitivity of 1.6 nm/kPa and a resonant frequency of 1.44 MHz. This sensor has potential applications in many fields such as structural health monitoring and medical ultrasonography.

Acknowledgement

The research in this thesis was carried out during my graduate study in the Department of Electrical Engineering at the University of Nebraska - Lincoln. Many people helped me to complete this work. First, I would like to express my gratitude to my thesis adviser, Professor Ming Han, who has a solid background in electrical engineering and wide research experience. I thank him for giving me a chance to work with him and for his continued support, valuable advice and encouragement.

I am grateful to Professors Dennis Alexander and Jinsong Huang for being my committee members; as well as Professors Yongfeng Lu and Mathias Schubert for their help.

I would like to take this opportunity to thank my colleagues in this group for being supportive all the time, Tongqing Liu, Qi zhang, and Tom Fink. Special thanks go to Tom Fink, Lucas Koester, and Professor Joseph Turner for their help during the ultrasonic measurement.

I would also like to thank my family for everything they have done for me.

This work was supported by Office of Naval Research under Grant N000141110499.

Table of Contents

LIST OF FIGURES

Chapter 1 Introduction

1.1 Background and Motivation

1.1.1 Background

Fiber-optic sensors can be used to measure a wide range of physical parameters, such as strain, temperature, pressure and other quantities by recording the changes in light intensity, phase, polarization or wavelength caused by these parameters in the fiber[1-6]. Compared to their electronic counterparts, fiber-optic sensors can provide numerous advantages. They are electromagnetically passive and immune to electromagnetic interference, which make them suitable for operation in environments with high and variable electric field [3]. They are made from silica glass so they are chemically and biologically inert. Also, the small size of optical fibers, generally on the order of hundreds of micrometers in diameter, makes the fiber-optic sensors physically small and light in weight. They can also perform distributed measurement, in which the measurand can be determined as a function of position along the length of a fiber or at a number of pre-selected locations of the fiber. The sensors can be interrogated from one end of the fiber[7-9]. Additionally, the long distance transmission capability of optical fiber enables remote sensing; the parameters being measured can be kilometers away from the monitoring station[10-12].

1.1.2 Fabry-Pérot Interferometer

The Fabry-Pérot interferometer (FPI), named after French physicists Charles Fabry and Alfred Perot, is typically formed by two reflecting surfaces or mirrors. It has been utilized for sensing applications for a long time[13,14]. The interference is caused by waves successively reflected between the two parallel surfaces. Their capability of transferring wavelength encoded information into an intensity signal enables high sensitivity and fast speed sensing. With the development of optical fiber technology, researchers realize that the combination of optical fiber sensor technology and Fabry-Pérot interference theory can form a new type of fiber sensor with many advantages. Recent developments have enabled FPIs to be formed conveniently at the fiber end. The so called Fiber-tip FPI sensor combines the advantages of both optical fiber and Fabry-Pérot interferometer sensors[15,16], including high sensitivity, easy fabrication, small size and low cost. Fig.1.1 shows a typical structure of the fiber-tip FPI sensor.

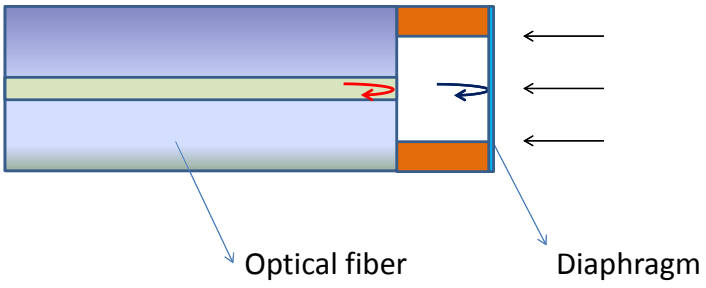

Figure 1.1 Fiber-tip FPI sensor

Several fabrication techniques for Fiber-tip sensors (FPI) using various film materials, such as silica[17], polymer[18] , pyrex[19], and graphene[20] , have been demonstrated in the

past few years. Most of them are based on silica film, which is obtained by splicing another piece of optical fiber to the fiber end face followed by cleaving[17,21-24]. These sensors have high temperature capability. However, due to the limited precision of the cleaving process, the film is typically tens of micrometers thick, which reduces the sensor sensitivity. Although hydrofluoric acid etching can reduce the film thickness and improve the sensitivity, it is still a big challenge to achieve the sub-micrometer thickness for silica film[21,25,26].

Polymers films fabricated onto the fiber tip from solutions also have been demonstrated[18,27-29]. They are usually a few micrometers thick. The thermal and chemical instability of the polymer film have limited their applications. Recently, a Fabry-Pérot fiber sensor based on an ultra-thin silver film on the order of 100 nm was reported for high sensitivity pressure measurement sensor[30]. The film was prepared by solution based silver mirror reaction and was absorbed to the end face of a fiber ferrule. This film preparation method is limited to the silver material. Furthermore, the sensor size is much larger than the fiber diameter due to the use of a fiber ferrule and thus cannot be considered as a true fiber-tip sensor.

1.1.3 Motivation

Miniature pressure sensors have been pursued in many fields, especially for medical applications, for example, in the development of minimally invasive surgical tools. More and more medical procedures are benefiting from these miniature pressure

sensors[31]. Such optical fiber sensors can be positioned at the tip of instrumented catheters to give useful feedback during surgical process.

Optical fiber sensors have been used for the direct visualization of the gastrointestinal tract, bronchial system, and vasculature through natural body orifices or small incisions[32]. Taking these advantages, physicians are able to reduce patient trauma, decrease surging time, and accelerate recovery.

Invasive pressure measurement, such as monitoring of arterial or venous blood pressure, coronary, pulmonary and intracranial pressure measurements, is another potential application of these miniature pressure sensors. Today's most invasive pressure measurements use fluid filled catheter that transfers measured pressure to external transducer. However, its bulky size makes it very difficult to apply in small blood vessels.

Current studies of Fiber-tip sensors with silica or metal films usually have a thickness of several micrometers, which limits their sensitivity. A film with thickness in the range of hundreds of nanometers is preferred for this kind of fiber-tip sensor. It is still a big challenge to get fiber-tip sensors with precisely-controlled film thickness below hundreds nm. A new structure and new fabrication method is in need to obtain high sensitivity and small size fiber-tip sensors with ultra-thin diaphragms.

In this thesis, a novel fabrication method to get fiber-tip sensors with film thickness in the range of nanometers was proposed. The proposed fiber-tip Fabry-Pérot interferometer has small size and high sensitivity, which makes it a perfect candidate

for medical applications, such as non-invasive pressure measurement and ultrasonic testing.

1.2 Tasks of Current Research

The tasks in this thesis include:

1. Develope a proper fabrication method for fiber tip-sensors based on thin metal films; with thickness of hundreds nanometers; and
2. Study the performance of the as fabricated fiber tip-sensors, including sensitivity, linearity, and stability, in both static pressure measurement and ultrasonic measurement.

1.3 Thesis Outline

In this thesis, a miniature optical fiber tip pressure sensor with a diameter of 125 μm was proposed and fabricated; the static pressure and ultrasonic response were also studied.

This thesis is organized into five chapters.

Chapter 1: Introduction. This chapter covers the backgrounds and motivations of the fiber-tip sensors and an outline of this thesis.

Chapter 2: Fiber-tip sensor design. This chapter describes the considerations for the sensor design for enhanced sensitivity and frequency response.

Chapter 3: Fabrication of Fiber-Tip sensors. This chapter presents the fabrication process of the fiber-tip sensor.

Chapter 4: Sensor characterization and test. The sensor's static and dynamic pressure performance is measured and analyzed, including sensitivity, linearity, stability, and frequency response.

Chapter 5: Conclusions and future work. This chapter summarizes this thesis and also provides some suggestions for future research.

Chapter 2 Design of Fiber-Tip Sensors

Fiber-tip pressure sensors have attracted a great deal of interesting attention recently. These devices are usually manufactured with rectangular or circular films with thickness in the order of micrometers. The development of a high-performance thin film structure is of critical importance in realizing these sensors. Thin film with linear deflection is needed in these pressure sensors. In order to increase the sensitivity, the film thickness should be thin to maximize the deflection responses. However, the thin film also leads to lower resonant frequencies. In order to have a flat response in the interested frequency range, the upper limit of the measured frequency needs to be much lower than the lowest resonant frequency of the sensor. In addition, the size of the diaphragm also has a significant effect on the sensitivity and frequency response of the sensor. Therefore, it is important to study the relationship between the film structure (thickness, radius, and material properties) and sensor performance (sensitivity and frequency response).

2.1 Thin Film Pressure Response

One common way to study the elastic properties of thin films is the load-deflection method[33]. In this technique, the deflection of a suspended film is measured under the applied pressure. The two typical shapes, round and square are discussed in the following part, respectively.

2.1.1 Round Shape Thin Film

For the clamped round shape thin film on the fiber tip, it can be deflected under a uniform pressure *P*. As shown in Fig.2.1.

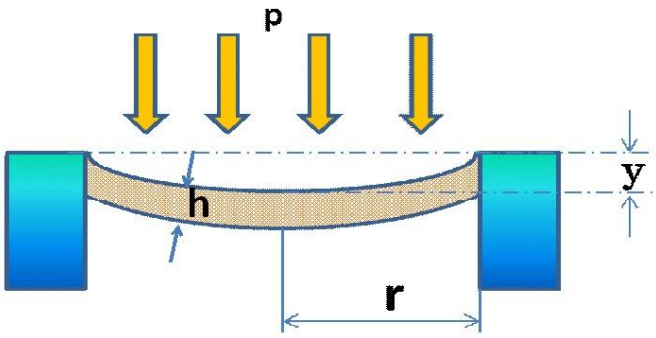

Figure 2.1 Deflection of round shape film under pressure

The center deflection of the round film *y* is a function of the pressure given by[34]

$$y = \frac{3(1-\nu^2)P}{16Eh^3}r^4 \quad (1)$$

Where *y* = deflection of the film

P = pressure

h = film thickness

r = effective film radius

E = Young's Modulus. The average value of Young's Modulus for bulk silver is 83 GPa[35].

ν = Poisson's Ratio. When an object is stretched or squeezed, to an extension or contraction in the direction of the applied load, it will induce a contraction or extension in the direction perpendicular to the applied load. Poisson's Ratio is the ratio between these two quantities. Most materials have

Poisson's ratio values ranging between 0.0 and 0.5[36]. Silver has a Poisson's ratio of 0.367[37].

Eq. (1) is valid only if the deflection is smaller than 30% of the film thickness and the thickness of the film should not be more than 20% of the diameters. For any given fiber-tip sensor, it has a finite pressure measurement range which is determined by the thickness and radius of the film, young's modulus and poisson's ratio of the materials. The maximum measurable pressure with linear response can be calculated by[34]

$$p < \frac{8\mathrm{Eh}^3}{5(1-\nu^2)\mathrm{r}^4} \tag{2}$$

2.1.2 Square Shape Thin Film

The load-deflection relationship for square films can be expressed by[38]

$$\frac{Pa^4}{Eh^4} = \frac{4.2}{(1-\nu^2)}\left[\frac{y}{h}\right] + \frac{1.58}{(1-\nu)}\left[\frac{y}{h}\right]^3 \tag{3}$$

Where P is the applied pressure (Pascal)

y is the center deflection of the film

a is the half side length

h is the thickness of the film

Eq. (3) includes a linear term and a non-linear cubic term of y, which describe two different deflection ranges, respectively. The linear term describes the relationship when the deflection is less than 25% of the film thickness; the non-linear term related with a deflection larger than 25% of the film thickness.

There is a general rule for the film design: for a linearity better than 0.3%, the maximum deflection of the film at the center part should be limited to one quarter the film thickness[39].

For the linear term in Eq. (3),

$$y = \frac{pa^4(1-\nu^2)}{4.2Eh^3} \quad (4)$$

In conclusion, the deflection change, i.e., the gap change between the fiber end and the thin film, is linearly dependent on the applied pressure. Resolving the deflection change from the spectral shift can provide information about the pressure[40].

It can be seen from Eqs. (1) and (3), both for round shape film and square shape thin film, that the maximum pressure can be greatly improved by increasing the thickness and/or decreasing the size (radius or length) of the film.

2.1.3 Sensitivity

Sensitivity (δ), defined by the ratio of the deflection to the pressure applied,[41,42] is one of the most important performance parameters of a pressure sensor.

For a round shaped film, the sensitivity is given by[34]

$$\delta = \frac{3(1-\nu^2)}{16Eh^3} r^4 \quad (5)$$

The sensitivity is highly dependent on the film's thickness and radius. When the thickness is fixed, the sensitivity increases with increasing film radius. Fig 2.2 shows the relationship between the sensitivity and radius when using silver film with a fixed thickness of 300 nm.

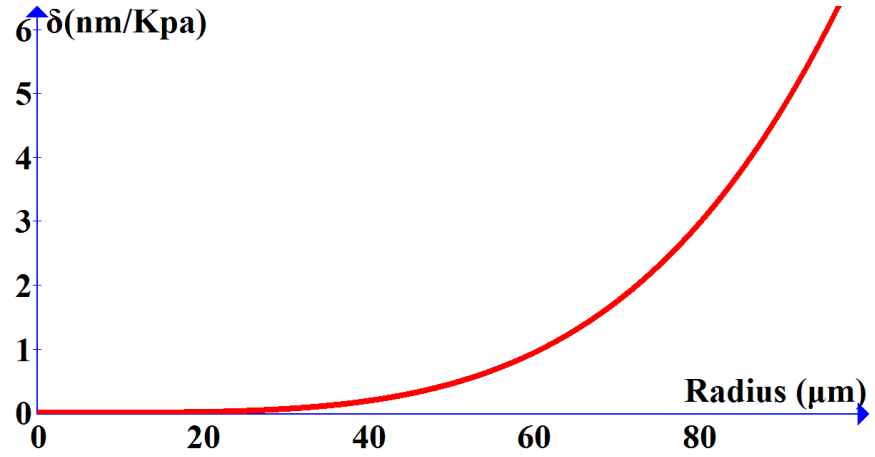

Fig 2.2 Sensitivity versus radius under a fixed thickness of 300 nm (silver film)

When the radius is fixed, the sensitivity decreases as the thickness increases, as show in Fig 2.3. Therefore, with thinner and larger film, high sensitivity can be obtained.

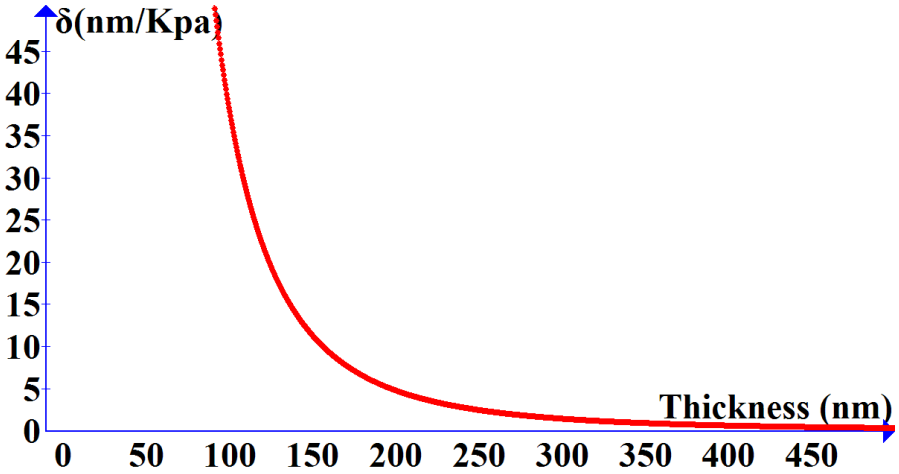

Figure 2.3 Sensitivity versus thickness under a fixed radius of 38 μm (silver film)

2.2 Film Frequency Response

The film frequency response is also an important consideration regarding the sensor design, especially when the sensors are designed for ultrasonic/acoustic measurement. In order to achieve good linearity of the sensor responses to the applied pressure, the signal frequency needs to be much smaller than the lowest resonant frequency of the diaphragm structure.

2.2.1 Round Shape Thin Film

Assume the film act as a free vibrating circular plate clamped rigidly at the edge. Its lowest resonant frequency f_0 is expressed as follows:[34]

$$f_0 = \frac{10.21}{4\pi}\frac{E}{3\rho(1-\nu^2)}\left(\frac{h}{r^2}\right) \quad (6)$$

Where h is the thickness of the film

r is the effective film radius

ρ is mass density of the film material

ν is the Poisson's ratio

E is the Young's modulus of the film material.

Fig 2.4 shows the relationship between the lowest resonant frequency and the radius of a silver film with a fixed thickness of 300 nm. It can be seen that a small radius is needed to get a high resonant frequency.

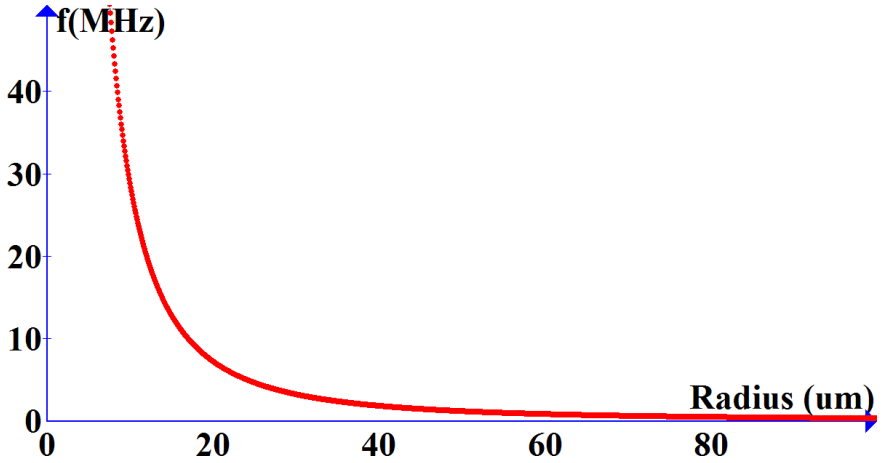

Figure 2.4 The lowest resonant frequency versus radius under a fixed thickness of 300 nm (silver film)

The relationship between the lowest resonant frequency and the thickness of a silver film with a fixed radius of 38 μm is also shown in Fig 2.5. They have a linear relationship, the lowest resonant frequency increases with thickness.

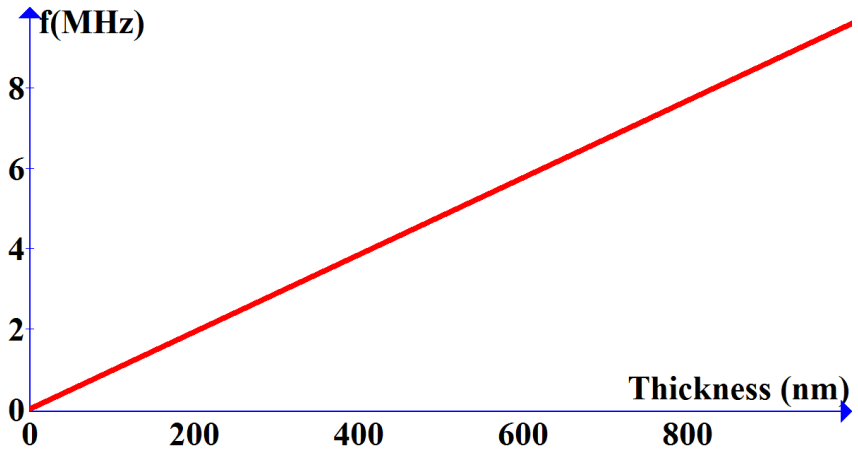

Figure 2.5 The lowest resonant frequency versus thickness with a fixed radius of 38 μm (silver film)

2.2.2 Square Shape Thin Film

Assuming that the deflection of the thin film is small compared to its thickness. The Reyleigh-Ritz method can be used to find the frequency of the lowest mode of vibration for square-shaped thin film [34]. The fundamental frequency for a square plate having density ρ and oscillating in a medium with density ρ_m can be expressed by:

$$f_1 = \frac{10.21}{a^2\sqrt{1+ß}}\sqrt{\frac{gD}{\rho h}} \tag{7}$$

Where g is acceleration of gravity, ß and D is given by

$$ß = 0.6689\frac{\rho_m}{\rho}\frac{a}{h} \tag{8}$$

$$D = \frac{Eh^3}{12(1-\nu^2)} \tag{9}$$

Where a is the half side length, h is the thickness of the film.

2.3 Film Thickness and Radius Considerations

As shown in Eq. (3) and (7), high frequency response and high sensitivity are two opposing requirements for the thin film. The frequency response is proportional to the thickness and inversely proportional to the square of the radius. Generally, in order to obtain a flat response within a specific frequency range, the working frequency should be far lower than the lowest resonant frequency. In order to measure dynamic pressure at high frequency, a thin film with high natural frequency is needed. In this case, a thicker and smaller film is preferred. This is contrary to the requirement of high sensitivity. So there should be a tradeoff to design the film with a proper radius and thickness, depending on the application requirement. However, we show that any desired sensitivity and natural frequency can be simultaneously obtained by a film with appropriate thickness and size.

Let's consider a round thin film, for any given values of δ and $f_{0,}$ solving Eqs. (5) and (6), we get

$$h = 0.014 \frac{E}{\rho^2(1-\nu^2)} \frac{1}{\delta {f_0}^2} \tag{10}$$

$$r = 0.0611 \frac{E}{\rho^{1.5}(1-\nu^2)} \frac{1}{\delta^{0.5} {f_0}^{1.5}} \tag{11}$$

Eqs. (10) and (11) indicate that the sensitivity and response frequency can be simultaneously increased by reducing the thickness and radius of the film.

In order to design a high sensitivity pressure sensor for measuring static and dynamic pressure, the cavity length (the distance between the fiber and thin film), diameter and film thickness are three key parameters.

2.4 Material Selection

According to Eqs. (5) and (6), materials properties, such as Young's modulus, Poisson's ratio and mass density, will also affect the sensitivity and frequency response. However, these influences on the sensitivity and frequency are not as notable as the film radius and thickness. Fig 2.6 illustrates the relationship between sensitivity and Poisson's ratio based on the assumption that the young's modulus is a constant for different materials.

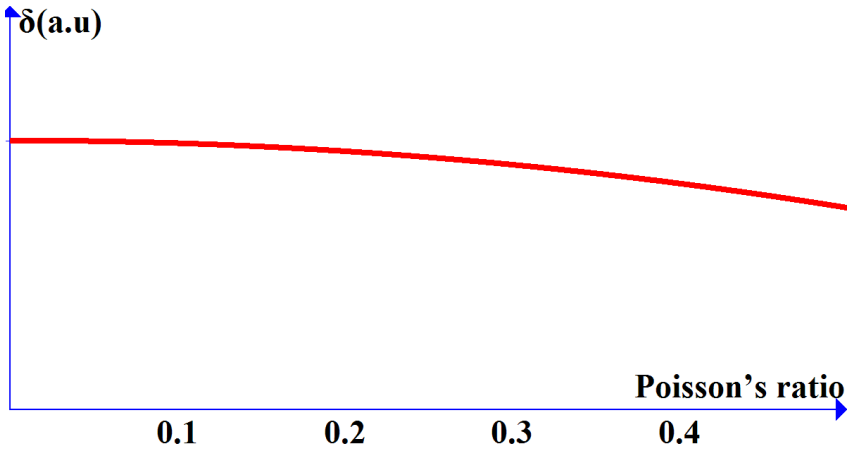

Figure 2.6 Effects of Poisson's ratio on sensitivity

With thermal evaporation technology, many kinds of materials can be used to form the thin film, such as aluminum, copper, silver, and gold. In this thesis, silver was selected for the sensor fabrication.

Chapter 3 Fabrication of Fiber-Tip Sensors

The whole fabrication processes of the proposed Fiber-tip sensor has three separate steps, including (1) preparing the silver film; (2)forming the optical cavity; and (3) bonding the silver film to the cavity. These processes are sketched in Fig.3.1 and explained in details in this chapter.

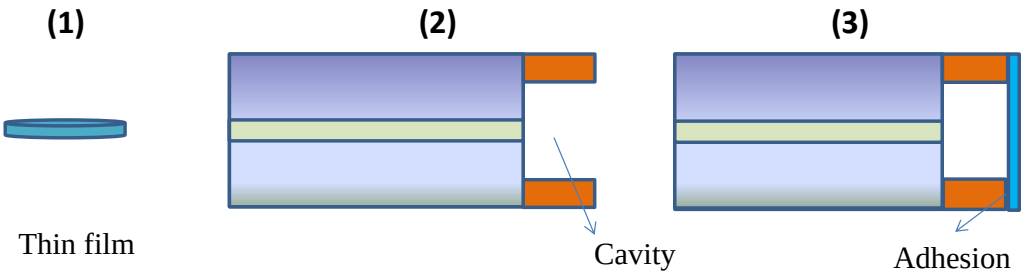

Figure 3.1 Fabrication processes of the Fiber-tip sensors

3.1 Silver Film Preparation

Silver thin film is deposited by vacuum thermal evaporation. Vacuum thermal evaporation is a common method of thin film deposition, and has found wide applications for organic electronic devices. The source material is heated and evaporated in a vacuum. The vacuum allows vapor particles to travel directly to the substrate, where they condense back to their solid state.

For the silver film deposition, bulk silver was put on the tungsten filament, and was heated to the point where the silver evaporates in vacuum. The silver vapor finally condenses in the form of a thin film on the cold glass substrate surface. Usually low pressure of 10^{-6} Torr is used to avoid reaction between the vapor and atmosphere. At these low pressures, the mean free path of vapor atoms is the same order as the

vacuum chamber dimensions, so these particles travel in straight lines from the evaporation source towards the substrate. The film thickness and deposition speed was monitored by a quartz crystal resonator simultaneously**.** A shadow mask was used between the substrate and the material source to form special shape of the thin films. In this thesis, A 300 nm thick silver films with round shape was deposited to fit the fiber head face. Fig.3.2 shows a sketch of the deposition process with a shadow mask. The evaporated silver particles were passing through the mask and directly condensed to solid state on the glass substrate.

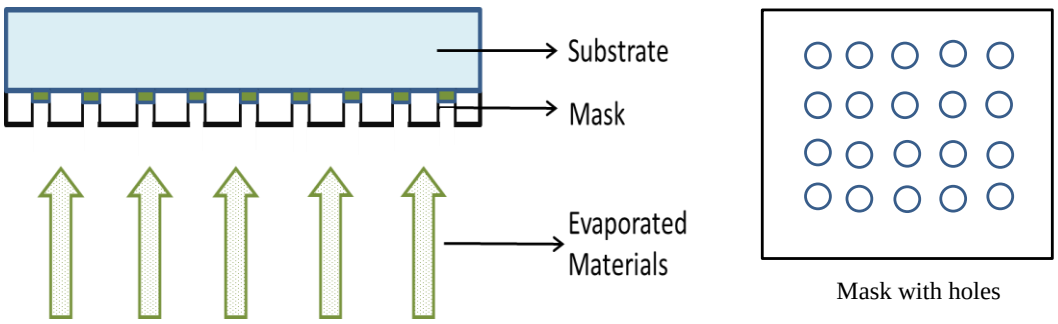

Figure 3.2 Sketch of the deposition process with a shadow mask inside a vacuum system

In order to get a more uniform silver film that can easily be peeled off from the substrate, an intermediate layer was deposited between silver and glass substrate, as shown in Fig.3.3 (a). A water-soluble material can be used for this purpose, such as lithium fluoride (LiF) and PEDOT:PSS. Here lithium fluoride was selected as the intermediate layer, which has a thickness of 100 nm by thermal evaporation. Fig.3.3 (b) shows the deposited silver film with different diameters on glass substrate. With this method, hundreds pieces of films can be obtained with one deposition process, which is suitable for mass production.

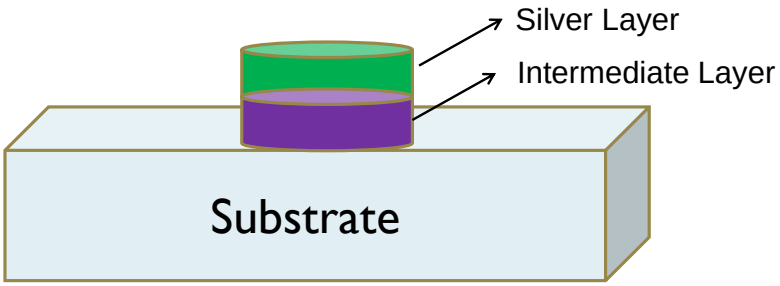

(a)

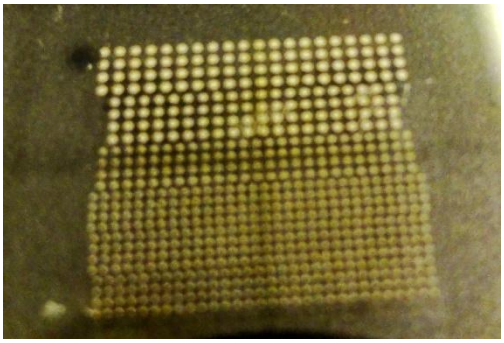

(b)

Figure 3. 3 Sketch of the intermediary layer (a) and picture of deposited silver with different diameters on glass substrate (b)

3.2 Cavity Formation

For the proposed Fiber-tip sensor fabrication, the general idea is to use a micro tube to connect the thin film and the fiber. The micro tube is a glass tube that has a diameter in the range of hundreds micrometers. Two different methods have been used to form the cavity at the tip of a fiber depending on the diameter of the micro tube.

3.2.1 First Method

In this method, the micro-tube used has an outside diameter of 365 μm and inside diameter of 150 μm. The fabrication process of the cavity was summarized as follows:

The protective plastic coating of the single mode fiber (SMF) was firstly removed and then the fiber was cleaved. After that the fiber was put into the micro-tube from one end. With the help of a microscope, the fiber was pushed slowly in to the tube and stopped when the proper distance between the tube and the fiber end surface was obtained. Then UV cure adhesive was used to bond the fiber with the tube. Finally, the cavity was obtained, as shown in Fig.3.4.

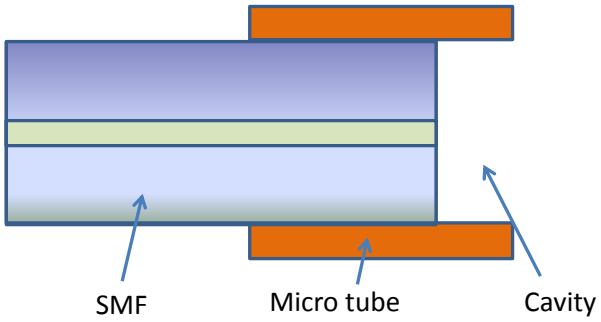

Figure 3.4 The formed cavity with micro tube by method 1

3.2.2 Second Method

In order to reduce the overall size of the sensor, a micro-tube that has the same outside diameter as the optical fiber was selected. The inner diameter of the tube used is 70 μm and the outside diameter is 125 μm.

First, the SMF fiber was spliced with the micro tube by fiber splicer in manual mode. With proper splice parameters, they can be spliced together without obvious damage to the fiber end surface. Then the tube was cut to the specified length with the help of a microscope. Fig 3.5 shows the cavity formed by this method.

Figure 3.5 The formed cavity with micro tube by method 2

3.3 Adhesion process

The adhesion process is aims to attach the silver films to the fabricated cavity (the end surface of the micro tube). Epoxy UV cure adhesive was used to do the attachment. The micro tube was fixed on a stage and can move up and down with accurate control. The setup for this process includes a microscope and monitor, translational stage, and UV lamp, as shown in Fig 3.6.

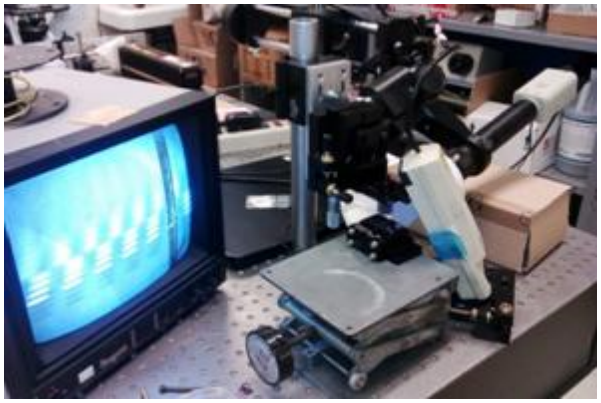

Figure 3.6 Setup for the adhesive process, includes microscope and monitor, translational stage, UV lamp

The adhesion process includes 3 steps, as shown in Fig.3.7 (1)-(3).

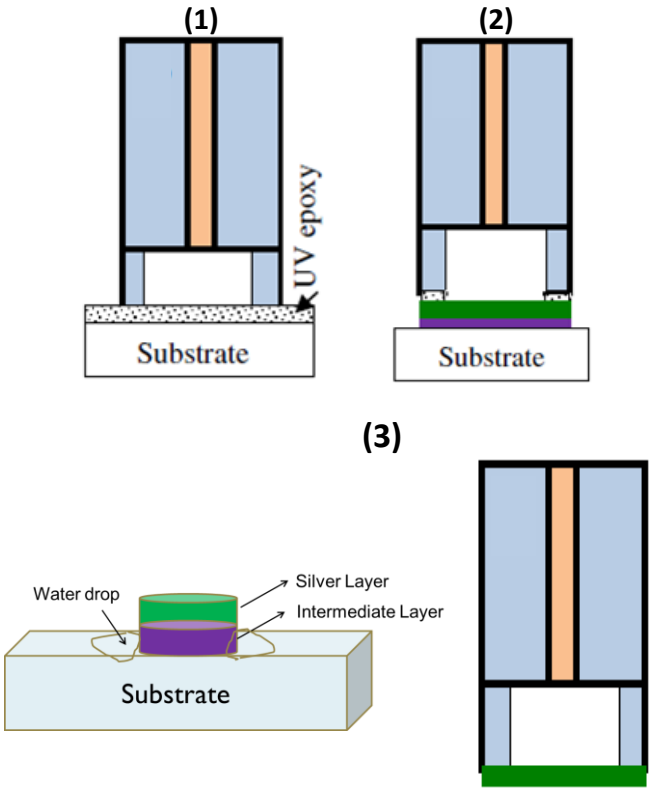

Figure 3.7 Sketch of the adhesive process: (1) attach the UV adhesive to the end surface of the cavity;(2) attach the silver film to the cavity; (3) peel off the silver film from the substrate.

Firstly, the adhesive was put onto the end surface of the tube. With the help of a microscope, the tube was moved down to the UV adhesive film, and after they touched with each other, the tube was lifted up. With this step, the UV cure adhesive can be successively attached to the end surface of the cavity, see Fig.3.7. (1) and Fig.3.8. In order to avoid the syphonage effect by the micro tube, the epoxy adhesive was spin coated on a glass substrate (4,000 rpm, for 1 min). Through spin coating, a uniform adhesive film can be obtained with a thickness of about 3 μm.

Secondly, the silver film was put under the micro tube and the tube was moved down again. Once they attached, a UV lamp was put aside to provide a UV irradiation to the adhesive for about 10 minutes (the needed time depends on the UV light intensity). Then the film was attached to the micro tube firmly, see Fig.3.7. (2) and Fig.3.9.

In the end, a drop of water was put on the substrate which will dissolve the intermediate layer of lithium fluoride, as shown in Fig.3.7. (3). The silver film then can be peeled off without any damage. Thus a Fiber-tip sensor has been fabricated. Fig.3.10 shows the fabricated fiber-tip sensors, on topside is the sensor with micro tube that has a larger diameter and the downside has a smaller diameter.

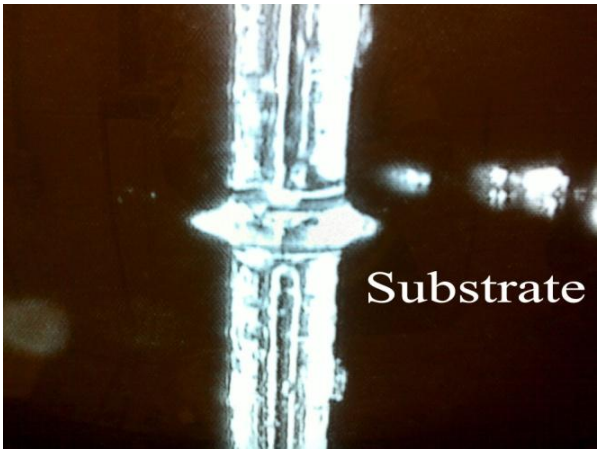

Figure 3.8 The adhesion process (1). This picture shows the micro tube cavity has been touched to the UV cure adhesion on the glass substrate.

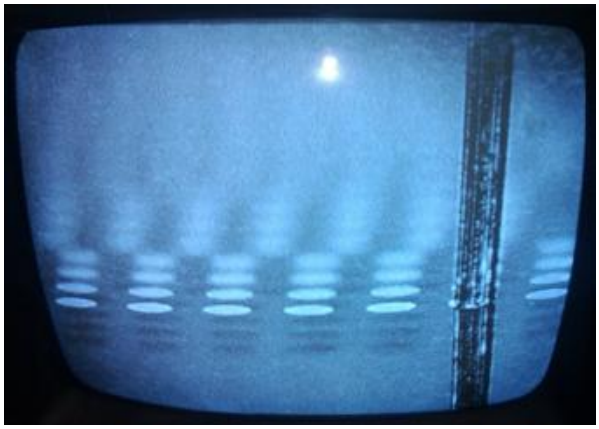

Figure 3.9 Monitor of Microscope, this picture shows the silver film was attached to the cavity at the fiber end

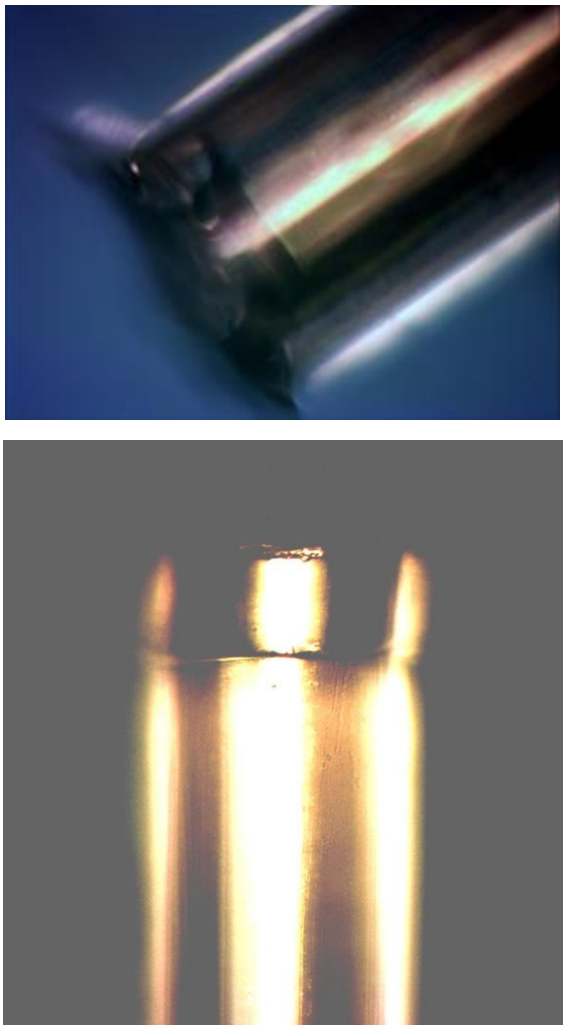

Figure.3.10 Pictures of the sensor made by the first method (upside) and second method (downside)

The whole fabrication process is summarized in Fig.3.11 (a)-(f)[43].

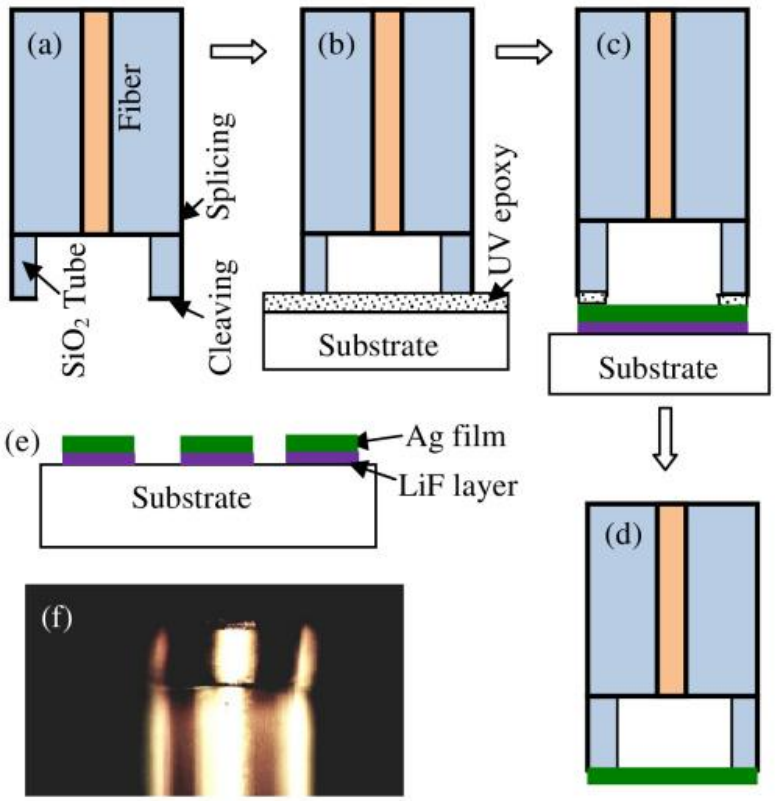

Figure 3.11 Sensor fabrication process (a)–(d), silver thin film deposited on a glass substrate (e), and an optical microscope picture (f) of a typical sensor fabricated

Chapter 4 Sensor Characterization and Test

4.1 Static Pressure Test

The sensor's response to static gas pressures was tested. Compressed liquid nitrogen (N_2) and a gas regulator were used to provide constant pressure for this measurement. The differential gas pressure is changed from 0 psi to 50 psi in steps of 10 psi. The fabricated sensor is put in a plastic tube; the gas pressure was applied through the other end of the plastic tube, as shown in Figs 4.1 and 4.2.

Figure 4.1 Measurement setup, includes air pressure source, Si125 interrogator, and computer

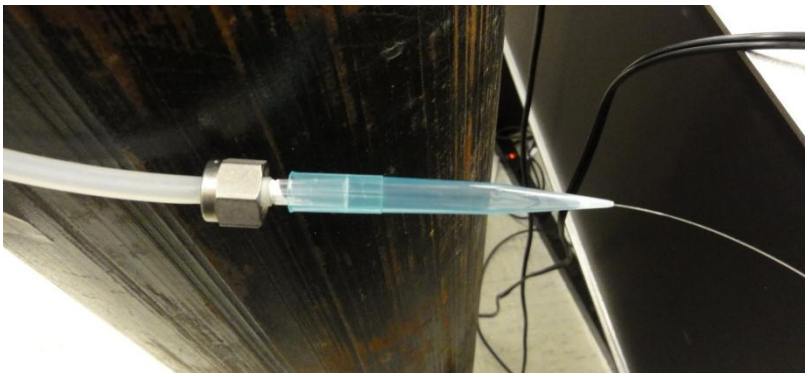

Figure 4.2 Sealed sensor under testing, the gas pressure was applied through the white plastic tube at the left side; the fiber-tip sensor is sealed in the blue plastic tube.

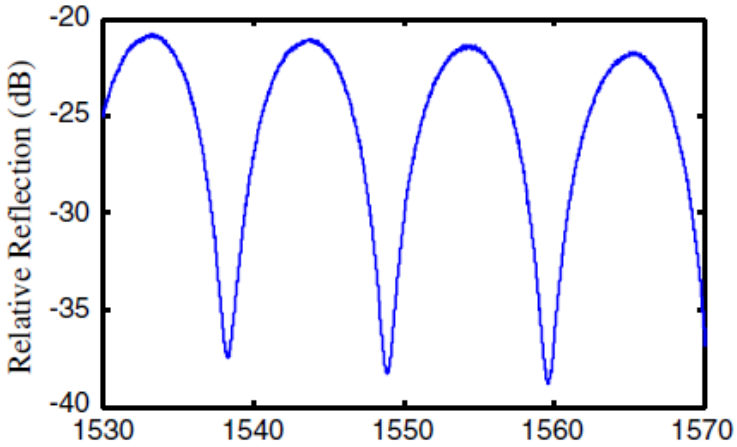

Figure 4.3 Result of two-beam interference of the Fiber-tip sensor

Fig.4.3 shows the reflection spectrum of a fabricated sensor measured by a sensor interrogator (Si125, Micro Optics). It is a result of two-beam interference. The cavity length *d* can be calculated by

$$d = \frac{\lambda^2}{2\delta\lambda} \tag{12}$$

Where λ is the dip wavelength, δλ is the wavelength spacing between two adjacent fringes. The sinusoidal interference fringes indicate that the FP cavity length is around 110 μm. Fig.4.4 shows the reflection spectrum of the fiber-tip sensor at different differential pressure levels measured by a sensor interrogator (Si125, Micron Optics). As expected, the fringes shifted toward the lower wavelength as the gas pressure increase deformed the film and reduced FP cavity length.

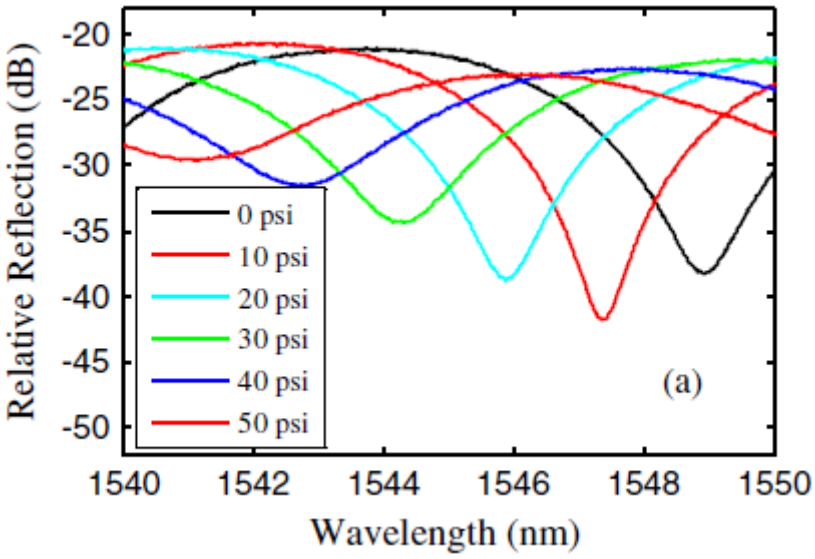

Figure 4.4 Reflection spectrum at different pressure levels

4.1.1 Linearity

The linearity is an important parameter for a sensor to detect a wide range of signal intensities. The linearity of the fiber-tip sensor is measured under different static gas pressures. The spectral valley in the range of 1540-1550 nm and its linear fitting curve as a function of differential pressure is shown in Fig.4.5. The linear fitting curve indicates that the fiber-tip sensor has a very good linear response to differential pressure, with a correlation coefficient (*R)* of 0.99989. From the FP cavity length and the linear fitting curve, the pressure sensitivity of the sensor is calculated to be approximately1.6 nm/kPa.

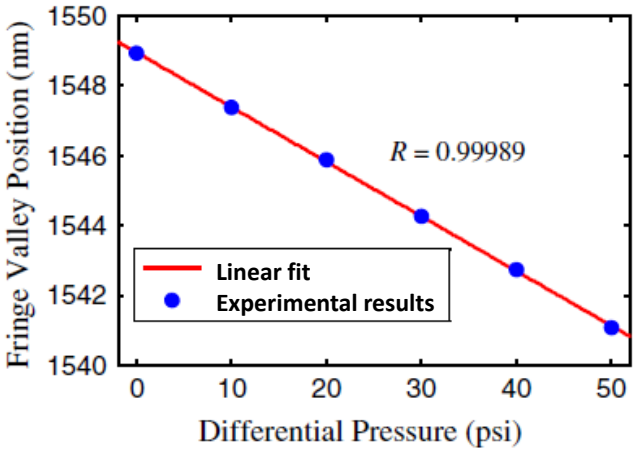

Figure 4.5 spectral position of the fringe valley vs. differential pressure

4.1.2 Stability

To check the stability, a constant pressure of 10 psi was applied to the sensor for up to 60 minutes and the results were recorded at 10, 30 and 60 minutes, respectively. As shown in Fig 4.6, the reflection spectrums show a slight shift (approximately 10%) to the short wavelength side after one hour. The reason for this shift is still unclear and needs to be further studied. However, one possible reason may come from the unstable air pressure source.

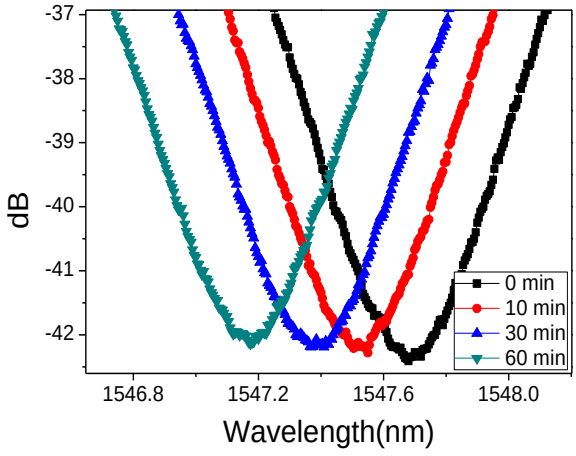

Figure 4.6 Stability of the sensor

4.2 Frequency Response Test

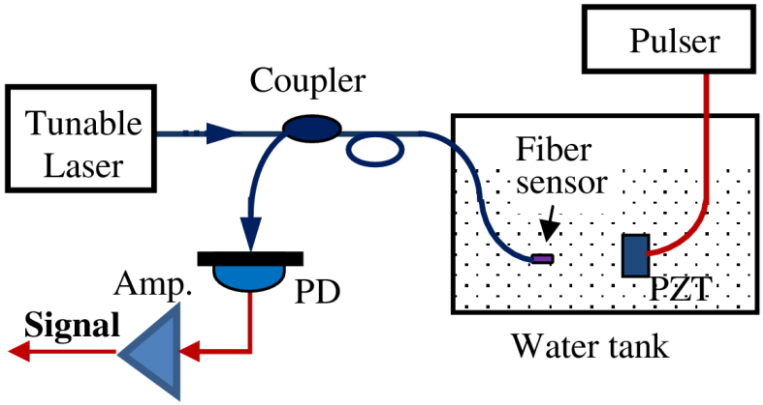

Figure 4.7 Setup for frequency response test of the fiber-tip sensor

In addition to the static pressure test, the impulse response of the same sensor was also characterized to an ultrasonic pressure field generated by an ultrasonic piezoelectric transducer (PZT) in water and then obtained the frequency response of the sensor by carrying out the Fourier transform of its impulse response. The experimental setup is schematically shown in Fig.4.7. A wavelength tunable laser was used as the light source, whose wavelength was tuned to a quadrature point of the reflection fringes of the sensor. The reflected light from the sensor was detected by a high speed photodetector followed by a band-pass amplifier. The amplification bandwidth of the amplifier is 20 KHz – 20 MHz. The PZT has a resonant frequency of 5 MHz and is powered by a pulser to generate an ultrasonic impulse. Fig 4.8a shows the ultrasonic generated impulse, which is measured by the same PZT using the "pitch-and-catch" mode through a point reflector placed at the center between the PZT and the fiber-tip sensor. It is seen that the ultrasonic pulse consisted of a few cycles of a 5 MHz signal. The pulse width, defined by the full-width-at-half-maximum (FWHM) of the ultrasonic envelope, is approximately

600 ns. Fig 4.8 b shows the response of the fiber-tip sensor to the ultrasonic impulse. The exponentially decreasing ringing signal typical to the impulse response of a resonator is evident in the figure. The frequency response of the sensor, given by the Fourier transform of the impulse response, is shown in Fig. 4.8 c. The resonant frequency of the fiber-tip sensor is 1.44 MHz and the 3-dB bandwidth of the frequency response is 0.10 MHz, from which the Q-factor of the film resonance is calculated to be 14.4[43].

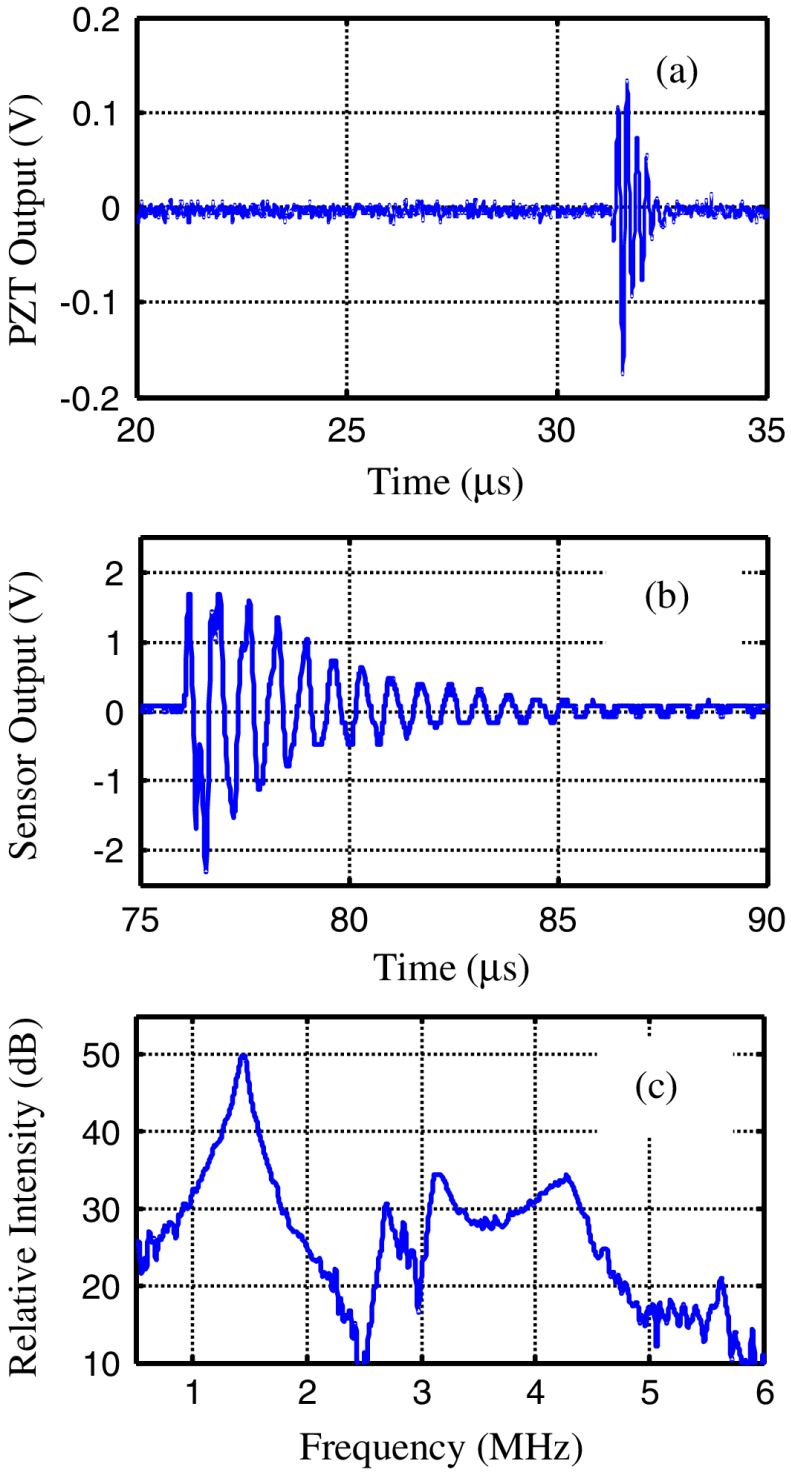

Figure 4.8 Frequency response test of the fiber-tip sensor : (a) ultrasonic impulse signal measured by the 5-MHz PZT; (b) Response of the fiber-tip sensor to the impulse pulse signal in (a); and (c) Fourier transform of the impulse response shown in (b).

Chapter 5 Conclusions and Future Work

5.1 Conclusions

1. A novel fabrication method for fiber-tip sensors based on an ultra-thin film have been proposed and experimentally demonstrated. The film is prepared by vacuum thin-film deposition technique and then transferred to a micro-tube that has been spliced to the fiber tip and cleaved to a desired length.
2. The fabrication method leads to ultra-thin and precisely controlled film thickness and many materials can be used for the film.
3. The transfer process of the silver film can also be used for other kind of films, such as polymers, and the films made by other methods.
4. The ultra-thin and ultra-small film renders a fiber-tip sensor with high sensitivity and high frequency response. The fiber-tip sensor demonstrated here has a 300-nm thick silver film on a 75-μm inner diameter micro-tube, which achieves a sensitivity of 1.6 nm/kPa and a resonant frequency of 1.44 MHz.

5.2 Future Works

1. The sensitivity and frequency response can be further improved by using thinner film and micro-tubes with smaller inner diameters.
2. Different materials, such as aluminum, gold, copper, and graphene for the thin film could be studied according to the requirements of unique applications.

3. Special optic fiber can be used to get unique fiber tip-sensors. For example, using fibers with side holes inside, additional pressure can be applied to the cavity through these holes to compensate the measured pressure. In this case, it can be used to measure ultrahigh pressure without damage to the fiber tip-sensor.
4. Most of the materials are temperature sensitive; their physical properties will change with the temperature shift. For example, the effects of thermal expansion should be considered when designing the fiber-tip sensor; the selected materials for the thin film could not have big difference in thermal expansion coefficient with that of the optical fibers. Temperature dependence on the performance, such as sensitivity and dynamic range, of the fiber-tip sensor should also be studied in the future.

References

1 Ferraro, P. & De Natale, G. On the possible use of optical fiber Bragg gratings as strain sensors for geodynamical monitoring. *Optics and Lasers in Engineering* **37**, 115-130 (2002).

2 Falciai, R., Mignani, A. & Vannini, A. Long period gratings as solution concentration sensors. *Sensors and Actuators B: Chemical* **74**, 74-77 (2001).

3 Wang, A. *et al.* Self-calibrated interferometric-intensity-based optical fiber sensors. *Journal of lightwave technology* **19**, 1495 (2001).

4 Rindorf, L. & Bang, O. Sensitivity of photonic crystal fiber grating sensors: biosensing, refractive index, strain, and temperature sensing. *JOSA B* **25**, 310-324 (2008).

5 Kersey, A. D. Optical fiber sensors for permanent downwell monitoring applications in the oil and gas industry. *IEICE TRANSACTIONS ON ELECTRONICS E SERIES C* **83**, 400-404 (2000).

6 Ohno, H., Naruse, H., Kihara, M. & Shimada, A. Industrial applications of the BOTDR optical fiber strain sensor. *Optical fiber technology* **7**, 45-64 (2001).

7 Juarez, J. C., Maier, E. W., Choi, K. N. & Taylor, H. F. Distributed fiber-optic intrusion sensor system. *Journal of lightwave technology* **23**, 2081 (2005).

8 Talaverano, L., Abad, S., Jarabo, S. & Lopez-Amo, M. Multiwavelength fiber laser sources with Bragg-grating sensor multiplexing capability. *Journal of lightwave technology* **19**, 553 (2001).

9 Sun, C. Multiplexing of fiber-optic acoustic sensors in a Michelson interferometer configuration. *Optics letters* **28**, 1001-1003 (2003).

10 Gianfrani, L., De Natale, P. & De Natale, G. Remote sensing of volcanic gases with a DFB-laser-based fiber spectrometer. *Applied Physics B: Lasers and Optics* **70**, 467-470 (2000).

11 Han, Y. G., Tran, T., Kim, S. H. & Lee, S. B. Development of a multiwavelength Raman fiber laser based on phase-shifted fiber Bragg gratings for long-distance remote-sensing applications. *Optics Letters* **30**, 1114-1116 (2005).

12 Han, Y. G., Tran, T., Kim, S. H. & Lee, S. B. Multiwavelength Raman-fiber-laser-based long-distance remote sensor for simultaneous measurement of strain and temperature. *Optics Letters* **30**, 1282-1284 (2005).

13 Hernández, G. *Fabry-Perot Interferometers*. (Cambridge Univ Pr, 1988).

14 Wei, T., Han, Y., Li, Y., Tsai, H. L. & Xiao, H. Temperature-insensitive miniaturized fiber inline Fabry-Perot interferometer for highly sensitive refractive index measurement. *Optics Express* **16**, 5764-5769 (2008).

15 Jiang, M. & Gerhard, E. A simple strain sensor using a thin film as a low-finesse fiber-optic Fabry-Perot interferometer. *Sensors and Actuators A: Physical* **88**, 41-46 (2001).

16 Choi, H. Y. *et al.* Miniature fiber-optic high temperature sensor based on a hybrid structured Fabry–Perot interferometer. *Optics Letters* **33**, 2455-2457 (2008).

17 Wang, X., Xu, J., Zhu, Y., Cooper, K. L. & Wang, A. All-fused-silica miniature optical fiber tip pressure sensor. *Optics Letters* **31**, 885-887 (2006).

18 Cibula, E. & Đonlagic, D. Miniature fiber-optic pressure sensor with a polymer diaphragm. *Applied optics* **44**, 2736-2744 (2005).

19 Saran, A., Abeysinghe, D. C. & Boyd, J. T. Microelectromechanical system pressure sensor integrated onto optical fiber by anodic bonding. *Applied optics* **45**, 1737-1742 (2006).

20 Ma, J., Jin, W., Ho, H. L. & Dai, J. Y. High-sensitivity fiber-tip pressure sensor with graphene diaphragm. *Optics Letters* **37**, 2493-2495 (2012).

21 Donlagic, D. & Cibula, E. All-fiber high-sensitivity pressure sensor with SiO2 diaphragm. *Optics letters* **30**, 2071-2073 (2005).

22 Zhu, Y. & Wang, A. Miniature fiber-optic pressure sensor. *Photonics Technology Letters, IEEE* **17**, 447-449 (2005).

23 Lin, V. S. Y., Motesharei, K., Dancil, K. P. S., Sailor, M. J. & Ghadiri, M. R. A porous silicon-based optical interferometric biosensor. *Science* **278**, 840-843 (1997).

24 Jerman, J., Clift, D. & Mallinson, S. A miniature Fabry-Perot interferometer with a corrugated silicon diaphragm support. *Sensors and Actuators A: Physical* **29**, 151-158 (1991).

25 Wang, W., Wu, N., Tian, Y., Niezrecki, C. & Wang, X. Miniature all-silica optical fiber pressure sensor with an ultrathin uniform diaphragm. *Optics Express* **18**, 9006-9014 (2010).

26 Cibula, E., Pevec, S., Lenardic, B., Pinet, E. & Donlagic, D. Miniature all-glass robust pressure sensor. *Optics Express* **17**, 5098-5106 (2009).

27 Chen, L., Chan, C., Yuan, W., Goh, S. & Sun, J. High performance chitosan diaphragm-based fiber-optic acoustic sensor. *Sensors and Actuators A: Physical* **163**, 42-47 (2010).

28 Beard, P. & Mills, T. Extrinsic optical-fiber ultrasound sensor using a thin polymer film as a low-finesse Fabry-Perot interferometer. *Applied optics* **35**, 663-675 (1996).

29 Beard, P. & Mills, T. Miniature optical fibre ultrasonic hydrophone using a Fabry-Perot polymer film interferometer. *Electronics Letters* **33**, 801-803 (1997).

30 Xu, F. *et al.* High-sensitivity Fabry–Perot interferometric pressure sensor based on a nanothick silver diaphragm. *Optics letters* **37**, 133-135 (2012).

31 Pinet, É. Medical applications: saving lives. *Nature photonics* **2**, 150-152 (2008).

32 Krohn, D. Fibre Optic Sensors, Fundamentals and Applications, Instrument Society of America. *Research Triangle Park, NC* **19912** (2000).

33 Tabata, O., Kawahata, K., Sugiyama, S. & Igarashi, I. Mechanical property measurements of thin films using load-deflection of composite rectangular membranes. *Sensors and Actuators* **20**, 135-141 (1989).

34 Di Giovanni, M. *Flat and corrugated diaphragm design handbook*. (CRC, 1982).

35 Wu, B. *et al.* Microstructure-hardened silver nanowires. *Nano letters* **6**, 468-472 (2006).

36 http://en.wikipedia.org/wiki/Poisson's_ratio.

37 Gercek, H. Poisson's ratio values for rocks. *International Journal of Rock Mechanics and Mining Sciences* **44**, 1-13 (2007).

38 Kovacs, G. T. A. *Micromachined transducers sourcebook*. (WCB/McGraw-Hill New York, NY, 1998).

39 Wang, X. *et al.* A New Method to Design Pressure Sensor Diaphragm. *SIMULATION* **2**, 112 (2004).

40 Françon, M. Optical interferometry. *New York: Academic Press, 1966* **1** (1966).

41 Timoshenko, S., Woinowsky-Krieger, S. & Woinowsky, S. *Theory of plates and shells*. Vol. 2 (McGraw-hill New York, 1959).

42 Soedel, W. *Vibrations of shells and plates*. (CRC, 2004).

43 Guo, F. *et al.* High-sensitivity, high-frequency extrinsic Fabry–Perot interferometric fiber-tip sensor based on a thin silver diaphragm. *Optics letters* **37**, 1505-1507 (2012).